Effects of Cyclohexane- Monoxime and Dioxime on the Electrodeposition of Cobalt

T. W. Lyons[a], Q. Huang[a,b,z]

[a.] *Department of Chemical and Biological Engineering,* [b.] *Center of Materials for Information Technology, University of Alabama, Tuscaloosa, 35487*

[z.] *corresponding author, email: qhuang@eng.ua.edu*

Abstract

Electrodeposition of cobalt was studied in presence of two additives, cyclohexane oxime (CHO) and cyclohexane dioxime (CHD), which differ by one oxime group. Cyclic voltammetry (CV), potentiostatic deposition with pulsed rotation rates, and galvanostatic deposition with injections of additives were carried out to understand the formation and breakdown of intermediate species that suppress cobalt electrodeposition. While strong and fast suppression was observed for CHD on cobalt deposition, the suppression effect of CHO was much less pronounced. A negative differential resistance in CV was observed for CHD due to a breakdown of suppression, which was related to the reduction of absorbed Co-CHD chelate species. A critical rotation rate was defined for CHD as the minimum rotation required to enable a fully suppressed deposition state. An inversely proportional relation between additive concentration and the square root of critical rotation rate demonstrated an equilibrium between the diffusion of the intermediate in solution and the consumption of intermediate by incorporation into deposit. While a pair of adjacent oxime groups was necessary for a strong fast suppression effect, bulkier molecular structures and stronger chelating resulted in stronger suppression.

1. Introduction

Copper back-end-of-line (BEOL) interconnect was invented in late 1990's[1,2] and has been used ever since for its superior conductivity, reliability and scalability. However, as the

dimension of interconnect structures approaches or even falls below the electron mean free path of copper, the copper resistivity in such very fine structures exponentially increases[3-8]. This is because electron scattering at interfaces between copper and surrounding materials and at grain boundaries can occur more often than the intrinsic electron scattering and dominate the material resistivity. Therefore, materials with much shorter electron mean free path are of interest[9] because of the insensitivity to scaling even if they have a higher bulk resistivity than copper. Among a list of candidate materials, cobalt has been identified as a front runner[10,11] because of its very short mean free path and relatively low cost.

Electrodeposition of copper interconnects has been studied for more than a decade and the mechanism of a so-called super conformal electrodeposition (or superfilling) has been well understood[12-14]. A preferential deposition at the bottom of a trench results in the defect free formation of interconnect structures. Superfilling of copper are generally accepted as a result of a synergistic interaction of two organic additives during copper electrodeposition[12-19]. An accelerator promotes the deposition rate at the bottom of the trench with respect to the top, where the rate is suppressed by a suppressor. A concentration gradient of suppressor can be present across the depth of the trench, resulting in a lower concentration of suppressor to facilitate the accelerator at the bottom of the trench[19-22]. Such synergistic mechanism between two-component additive system has been exercised for a few other metals[23-26].

On the other hand, a negative differential resistance (NDR), observed as an s-shaped cyclic voltammetry[27-30], has also been found to enable preferential deposition at the bottom of structures due to a positive feedback between deposition and adsorbate consumption (less suppression). Two stable steady states at a single deposition potential can be achieved in such

systems. Bottom up deposition in deep silicon via is a result of two different deposition steady states, i.e, fast deposition at the bottom and suppressed deposition at the top[30-32].

A list of different organic additives was previously studied for the superfilling of iron group metals in to sub-50 nm interconnect structures using NiFe as an example[33]. Nitrogen groups such as amine and imine were found to suppress the deposition rate whilst thiol groups to accelerate the deposition. A dioxime molecule, dimethylglyoxime (DMG), showed strong and fast suppressing effect on cobalt electrodeposition[34]. In addition, an agitation dependency of the suppression effect was observed, which is expected to potentially enable superconformal filling of cobalt interconnects.

This paper reports a study on the effects of steric structures of oxime molecules on the suppression effect of cobalt electrodeposition. Figure 1 compares the molecular structures of DMG and cyclohexanedione dioxime (CHD), which have two methyl groups and a 6-member alkyl ring, respectively. In addition, the role of the pairing of two dioxime groups are also studied with cyclohexane oxime (CHO), which is identical with CHD except for having only one oxime group.

2. Experimental

2.1 Electrochemical cell

A three-electrode cell with a glass frit to separate the cathode and anode solutions was used for the studies. A saturated calomel electrode (SCE) was used as a reference electrode and was placed in a compartment attached to that cathode via a capillary tube. All potentials were measured in reference to this SCE. The anode was a 99.95 at%. cobalt strip placed in the anolyte compartment. The cathode was a platinum rotating disk electrode (RDE) with 5 mm in diameter.

The RDE was pre-plated in a cobalt makeup solution before each experiment and was rotated at 100 rpm throughout the studies unless otherwise specified.

2.2 Materials

The cobalt makeup solution contains 0.3 M $CoSO_4$, 0.4 M H_3BO_3, and 0.1 g/L sodium dodecyl sulfate (SDS). The pH of Co solution was adjusted to 4.0 with H_2SO_4. Concentrated solutions of 0.1 wt% (1,000 ppm) CHO and of 0.7 wt% (7,000 ppm) CHD were prepared and added to the Co makeup electrolyte to a predetermined concentration. The studies were carried out using weight concentrations of additives. The molar weights of $–CH_2–$, –NH– or –O– groups are all similar and the total number of such groups are similar at a constant weight concentration of additive. A 0.2 M HCl solution was used to anodically strip the Co from the Pt RDE between each experiment. All salts and organic additives were at least ACS grade and deionized (DI) water with 18 MOhms were used in all experiments.

2.3 Procedures

The detailed experimental procedure of electrochemical studies was similar to a previous report for DMG[34]. A layer of about 100 nm cobalt was pre-plated using the makeup solution at -10 mA/cm^2 for 40 seconds. This cobalt layer is to eliminate the nucleation effect and keep substrate consistent among experiments. Cyclic voltammetry, chronopotentiometry with additive injections, and chronoamperometry with modulated agitations were carried out to understand the role of oxime groups. Impedance analysis was also carried out to measure the solution resistance, which was 53 ohm and did not change upon the addition of different additives. An Autolab 302N potentiostat was used for all the electrochemical studies.

3. Results and Discussion

3.1 Cyclic voltammetry

The effect of CHD on Co electrodeposition was first investigated with cyclic voltammetry (CV). The Pt RDE was pre-plated before each CV experiment with about 100 nm Co, which resulted in a change of open circuit potential from -0.3 V for Pt to -0.48 V for Co. The potential was therefore swept from -0.48 V to -1.5 V at a rate of 5 mV/sec. Figure 2(a) shows the CV results at different concentrations of CHD. A previous study on DMG showed that the partial current density of Co deposition was much more significant than the side reactions for the electrolytes used[34]. Therefore, CVs can be directly compared to show the effect of additives. Co deposition started at around -0.7 V with no CHD present and steadily increased to -1.5V. The addition of 10 ppm of CHD caused a suppression of Co deposition up to about -0.8V, below (less negative than) which no significant deposition occurred. A small hysteresis was observed on the reverse sweep, where deposition continued below -0.8 V. Increasing CHD concentration to 100 ppm increased the suppression potential to -1.0 V, where the suppression started to break down and deposition occurred. The deposition current density increased for more than 10 times, from -0.8 mA/cm^2 to -8.9 mA/cm^2, when the potential scanned from -1.01 to -1.05 V. In addition, the hysteresis in reverse sweep was much more pronounced as well. Increasing the CHD concentration to 300 and 500 ppm further increased the potential range of suppression up to -1.06 and -1.1 V, respectively. However, the deposition rate of cobalt after the suppression breakdown was still significantly lower than the case of 100 ppm CHD, resulting in much less pronounced hysteresis loops in CVs.

In addition to the suppression and suppression breakdown in cobalt electrodeposition, the current densities before the suppression breakdown also changed with the concentration of CHD. For example, the current density at -0.9 V was -0.42, -0.67, and -0.97 mA/cm^2 for 100, 300 and 500 ppm CHD, respectively. The increase of current density suggests an increasing catalytic effect of CHD on proton reduction reaction. Catalytic effects on proton reduction reaction have been reported widely on Co-dioxime type of molecules[35-38]. A surface adsorbed intermediate, for example $[Co(CHD)_2]_{ads}$, is typically involved in the facilitated charge transfer for proton reduction. Such an adsorbate is believed to result in the suppression of cobalt electrodeposition observed in this study.

The effect of CHO on Co deposition was studied in the same fashion. Figure 2(b) presents the CVs with different concentrations of CHO. The addition of 10 ppm of CHO was found to prevent deposition until a potential of -0.75 V as opposed to -0.7 V in CHO free deposition. The deposition was suppressed until -0.85 V at a concentration of 100 ppm. Not only was this suppression less pronounced than CHD, but also it saturated at a low concentration of 100 ppm and no further suppression was observed when more CHO was present. Furthermore, the cobalt deposition rates after the suppression breakdown were all comparable with the CHO free case and no significant differences were observed between different concentrations. In addition, whilst a small hysteresis was observed at 100 ppm CHO, no hysteresis was observed at concentrations beyond 100 ppm. The current trace on reverse scans precisely followed the forward scans, suggesting a much more sluggish breakdown or an extremely fast re-establishment of the weakly suppressing film on the electrode surface.

While CHD and CHO both suppressed the electrodeposition of cobalt, their suppression effects were obviously different. Figure 3 presents a comparison of the CVs of these two

additives with a third additive, DMG, which is a dioxime but smaller than CHD. The two polarization curves of DMG were adapted from a previous study[34]. The insets are the same CVs with potentials corrected for the solution resistance (53 ohm). The comparison was carried out using constant weight concentrations so that the total numbers of – CH_2 –, – NH – and – O – groups are similar for different molecules at a same weight concentration. At 100 ppm, all three additives showed suppression on cobalt deposition and the suppression effects all broke down. While cobalt deposition started at -0.7 V in absence of additives, it started at -0.84 V, -0.9 V and -1.01 V with 100 ppm CHO, DMG and CHD, respectively.

A first comparison between CHD and CHO showed that the presence of a second oxime group paired with the first oxime group on the organic molecule significantly enhanced the suppression effect. Another difference between these two molecules is the total number of alkyl groups (CH_2) in electrolyte when their weight concentrations were kept the same. Table 1 shows the molecular weights of the three additives as well as the molecular components, where 57% more (62% : 39%) CH_2 groups are expected for CHO than CHD. However, CHD also comprises 52% more (39% : 26%) CH_2 groups than DMG but it showed much more enhanced suppression than the latter. Therefore, the stronger suppression of CHD than CHO is believed due to the number of oxime groups. The pairing of the two adjacent oxime groups resulted in a much more pronounced suppression for CHD. This is also consistent with the much stronger suppression observed for DMG than CHO.

A second comparison between CHD and DMG shows the effect of steric structure of molecule. These two molecules both have a pair of oximes with the total number slightly greater for DMG than CHD at a constant weight concentration. But the suppression breakdown of DMG occurred at a much lower (less negative) potential than CHD. Furthermore, the current densities

before the suppression breakdown were approximately the same between the two additives. Therefore, a strongly suppressed state was believed to occur in both cases and the electrode surface was fully covered by chelated species such as $[Co(DMG)_2]_{ads}$ or $[Co(CHD)_2]_{ads}$. Cobalt electrodeposition rate was extremely slow under this situation. Considering the two mechanisms of the consumption of a typical adsorbed leveler[39], the different breakdown potentials of the two additives are believed to stem from the different potentials at which desorption or incorporation of the adsorbed species occurs.

The fact that the deposition currents after the suppression breakdown were the same as the additive-free solution suggest that the adsorbed $[CoL_2]_{ads}$ (L stands for ligand) completely disappeared within a narrow potential range. As the incorporation of adsorbates only occurs with cobalt deposition, this sudden breakdown is more likely initiated by a potential dependent decrease of surface coverage. However, once the deposition rate starts to increase, the increased incorporation of adsorbate further accelerated the breakdown of the suppression. On the other hand, the suppression effect was not re-established immediately when the potential reached the same range on the reverse sweep (Figure 2), consistent with the continuous incorporation of the adsorbate during electrodeposition. Therefore, the different molecular structures of DMG and CHD are believed to resulted in the different formation, initial breakdown and incorporation behaviors of the adsorbed chelate species.

At a higher concentration of 300 ppm the suppression effects were further different among these three additives. Cobalt deposition started at -0.87 V, -0.97 V and -1.07 V for CHO, DMG and CHD, respectively. While the order of these potentials was consistent with the cases of 100 ppm additives, the values were further apart. In addition, a suppression effect was observed for DMG and CHD even at highly negative potentials. The deposition current densities

with 100 ppm DMG, CHD or CHO increased rapidly after suppression breakdown and reached the same value as the additive free case. While this was still true for 300 ppm CHO, the presence of 300 ppm DMG or CHD consistently suppressed the deposition and shifted the CV curves for a constant voltage difference of -0.12 and -0.15 V, respectively. This voltage shift remained the same after the correction of solution resistance (inset).

In an electrodeposition system with a typical S-shaped NDR, the active deposition can be extremely local if the breakdown only starts at sporadic locations, resulting in a partial suppression effect on macroscopic observation. Such active spots can be surrounded by passivated areas with little or no deposition. The active deposition is typically further promoted due to the consumption of the adsorbate. Therefore, a so-called Turing pattern[40] can be observed resulted from the contrast between the fast deposition at one spot and the completely suppressed deposition around it[41]. Such patterns are typically observed at around the suppression breakdown potential, where multiple steady state conditions can be achieved at a single voltage. Cobalt films deposited on RDE with 300 ppm CHD or DMG at various potentials around the suppression breakdown were uniform and shiny (Supplementary Material Figure S.1). However, such absence of Turing patterns does not necessarily exclude the possibility of partial breakdown and its contribution to the constant shift of the CV curves in presence of CHD and DMG. On the other hand, a change of the redox speciation in electrolyte can result in a shift of redox potential as well. However, 300 ppm DMG or CHD is only equivalent to 2.5 or 2.1 mM. The latter are negligible compared with the 0.3 M Co^{2+} in electrolyte. The majority of cobalt in electrolyte was believed to be not complexed by dioxime.

In order to further understand the suppression breakdown at different potentials for different molecules, the reversible potentials (E_{rev}) for the reduction of chelate complexes were

calculated from the stability constants (pK_{st}). While such constants for Co^{2+} are not available, Table 1 presents the stability constants for Ni^{2+} chelates with CHD and DMG[42], which are believed to be similar to Co^{2+} chelates. The reduction reactions of bulk Co^{2+} and CoL_2 chelate are correlated through a complexing reaction as below, with L stands for ligands.

$$Co^{2+} + 2e \rightarrow Co \qquad \text{(Eq. 1)}$$

$$Co^{2+} + 2L^{-} \rightarrow CoL_2 \qquad \text{(Eq. 2)}$$

$$CoL_2 + 2e \rightarrow Co + 2L^{-} \qquad \text{(Eq. 3)}$$

The free Gibbs energy of the reactions follow the relation

$$\Delta G_{Eq.1} - \Delta G_{Eq.3} = \Delta G_{Eq.2} = -2.303 * RT * pK_{st}$$

therefore, at 20 °C

$$\Delta E_{rev} = E_{rev,Eq.3} - E_{rev,Eq.1} = -\frac{2.303 * RT * pK_{s.t.}}{2\ F} = -0.029\ pK_{st}\ (V)$$

Table 1 also lists the calculated shifts of reversible potentials (ΔE_{rev}) for the bulk $[Co(CHD)_2]$ and $[Co(DMG)_2]$ in electrolyte, which are -0. 62 and -0.5 V, respectively. While the difference of -0.12 V between the two is much larger than the difference in the bulk suppression effect of the additives (Figure 3b), it very well matches the difference in the breakdown potential of suppression effect at 100 ppm concentration (Figure 3a). This observation indirectly confirms that the suppression at low potential related to the adsorption to a chelate species and the breakdown of this suppression at higher potential was initiated by the reduction of this complexed species. Once the reduction starts the surface coverage of the chelate decreases and the cobalt deposition rate increases, which increases the incorporation of additive into the deposit and further decreases the surface coverage of the chelate. It should be noted that the adsorbed species typically have different reactivity from species in bulk electrolyte. In addition, the rate of adsorbate reduction is counter balanced by the rate of formation, which depends on the

concentration of additives. Therefore, the absolute values of the potentials are of less significance in this comparison and the difference between additives, i.e. CHD and DMG, was used to compare with calculation.

3.2 Mass transport effect

The cyclic voltammetry studies were carried out at a constant rotation rate of 100 rpm, which was expected to result in a constant diffusion flux of the additive species as they were consumed on the electrode. To investigate the effect of mass transport of additives on the suppression, potentiostatic cobalt electrodeposition was carried out on RDE with the rotation rates being varied. Figure 4(a) shows the study in presence of 100 ppm CHD at a potential of -0.95 V. The potential was chosen based on the CV in Figure 2(a), where a current hysteresis was observed between the forward and backward sweeps. A high current density at about -6.5 mA/cm^2 was observed in absence of agitation. The current dropped quickly to -1 mA/cm^2 when a rotation rate of 100, 200 or 400 rpm was applied, suggesting the formation of suppressing species, for example, $[Co(CHD)_2]_{ads}$, on the electrode surface. In addition, the deposition current did not increase to -6.5 mA/cm^2 immediately after the rotation was stopped. It further decreased before increasing back to the steady state at 0 rpm, suggesting a time delay for the consumption of excessive suppressing CHD species in the vicinity of electrode before the breakdown of suppression. The consumption is probably through the adsorption of $[Co(CHD)_2]_{bulk}$ onto electrode surface followed by the incorporation of $[Co(CHD)_2]_{ads}$ into deposit. This time delay increased with the rotation speed used, consistent with the thinner diffusion layer thickness and a higher surface concentration of $[Co(CHD)_2]_{bulk}$ at higher rotation speeds. While a fully suppression was also observed at a rotation of 77 rpm, it took longer time to reach the fully

suppressed state. In addition, the time delay of the current drop immediately after the rotation stopped was so short that it was barely observed. This is consistent with a critical rotation rate or critical supply rate of $[Co(CHD)_2]_{bulk}$, which is close to the rates of adsorption and incorporation. Therefore, the re-establishment of suppression was slow and there was little excessive $[Co(CHD)_2]_{bulk}$ near the electrode surface at steady state, resulting in an immediate current increase once the rotation stopped. At a rotation below this critical value, for example at 30 rpm, a partial suppression of cobalt deposition occurred because the supply rate of the $[Co(CHD)_2]_{bulk}$ to the surface was not fast enough to balance the incorporation of $[Co(CHD)_2]_{bulk}$ and to form a full surface coverage of suppressing film on electrode.

Subsequent experiments showed that this critical rotation rate depended on the applied voltages as well. For example, the critical value for agitation was found to be 200 rpm when the potential was lowered to -1.0 V and cobalt deposition was partially suppressed at 77 rpm. For an ideal isothermal electrochemical adsorption process, the adsorption and desorption rates are expected to depend on the additive concentration as well as the applied potential. Therefore, a change of applied potential shifts the equilibrium between adsorption and desorption. For the quasi-isothermal adsorption during electrodeposition, where the adsorbate also gets incorporated into deposit, a more negative potential resulted in a higher deposition rate and therefore a higher incorporation rate, further decreasing the surface coverage. A higher critical rotation rate was consistent with a hypothesized equilibrium between a faster supply rate of $[Co(CHD)_2]_{bulk}$ and a higher incorporation rate of $[Co(CHD)_2]_{ads}$ on electrode.

In order to further quantitatively examine this hypothesis, another study was conducted on the rotation rate effect with a lower concentration of CHD. An inverse relationship between critical rotation rates and additive concentrations was expected to exist at a constant potential.

Figure 2(b) shows the results of a study similar to Figure 2(a) at a same potential of -0.95 V but a lower CHD concentration of 71 ppm. The suppression re-establishment at 154 rpm was slower than at higher rotations and the time delay of the current decrease upon the stop of rotation was also barely observed, suggesting a critical rotation at around 154 rpm. As discussed above, supply rate of the $[Co(CHD)_2]_{bulk}$ to the electrode is in equilibrium with its consumption rate at critical rotation. The surface concentration is close to zero and the supply rate is proportional to the square root of rotation rate according to the Levich relation[43]. In other words, the supply rate of $[Co(CHD)_2]_{bulk}$ at 154 rpm would be $\sqrt{2}$ faster than at 77 rpm. However, the CHD concentration in the second study, 71 ppm, was decreased by a ratio of $\sqrt{2}$ from the first study in Figure 4(a), 100 ppm. Therefore, the effect of the 2X higher rotation rate was counter balanced by the decrease of bulk concentration, resulting in a same supply rate. A series of studies on this critical rotation rate is presented in Figure 4(c) and confirmed this hypothesized inversely proportional relationship between concentrations and the square root of critical rotation speeds.

While the current density observed at 0 rpm in Figure 4(b) was slightly lower than in Figure 4(a) due to experimental variation, the current densities at fully suppressed states or at high rotation rates are consistent between the two experiments. This probably corresponds to the similar consumption rate of $[Co(CHD)_2]_{ads}$ on the electrode surface between the two experiments, and a similar equilibrium state between supply and consumption.

Though the formation and breakdown of an adsorbed suppressing species may also apply for the suppression effect of CHO, it behaves differently than CHD. As shown in Figure 5(a), the current density that would stabilize at a voltage of – 0.85 V was directly correlated to the rotation rate. The higher the agitation rate the stronger the suppression. This is similar to the case of CHD. However, CHO differed in that the deposition rate varied without an obvious trend in

absence of agitation. A critical rotation rate could not be defined. In addition, a steady state current density of -1.3 mA/cm^2 was observed at 100 rpm in this study. On the other hand, the current density at the same rpm and same CHO concentration were -0.85 and -2.7 mA/cm^2 for the forward and backward sweeps in CV in Figure 1(a). All these differences seem to suggest a dependence of the current on the electrode history. In other words, the formation and/or consumption of the suppressing film on electrode may be extremely slow or insensitive to the agitation. This is also consistent with the fact that little difference was observed between the CVs with different concentrations of CHO in Figure 2(b).

At a lower (less negative) voltage of -0.815 V the relation between current density and rotation was completely different from the previous case at -0.85 V. Although a high deposition rate was observed at 0 rpm at the beginning, the current drops once rotation was turned on and the full deposition rate was never achieved again. The current density first dropped to -0.34 mA/cm^2 at a high rotation rate of 400 rpm presumably due to the formation of a suppression film on electrode. Once this rotation was stopped, the current further dropped to -0.03 mA/cm^2 due to a decrease of mass transport controlled reactions. The formation of suppression effect as well as this further decrease of current are both similar to the case of CHD. However, the current maintained at this extremely low value of -0.03 mA/cm^2 even 700 seconds after the rotation was stopped. The suppressing film did not break down and remained intact at this potential because no cobalt was electrodeposited under this condition and the suppressing adsorbate on the surface did not get incorporated. In other words, the current observed at this condition was 100% side reaction. A series of different rotation rates were applied and similar results were observed, resulting in a higher current density at a higher rotation rate. The insert in Figure 5(b) presents a

linear relation between the current densities and the square root of rotation rates [43], consistent with a mass transport limited side reaction.

Another set of studies on transport effects were carried out using cyclic voltammetry at different rotation rates. The results are presented in Figure 6. The CVs are in general of similar shapes as in Figure 2. In the case of CHD shown in Figure 6(a), when the rotation rate increased from 100 rpm to 900 rpm, the suppression breakdown potential slightly increased and behaved similar to the case where 300 ppm CHD was present but 100 rpm was used. In other words, the effect of increasing rotation for 9 times is similar to increasing concentration for 3 times. This is consistent with the observation and discussion in Figure 5, where an inverse relation was observed between the concentration and the square root of critical rotation rate due to the transport of CHD. On the other hand, no significant effect was observed for CHO when the rotation rate changes in Figure 6(b). This is also consistent with the little effect observed from the CHO concentration in Figure 2(b).

CVs at different rotation rates provide information of the transport effect for steady state or pseudo steady state electrodeposition at different potentials. On the other hand, galvanostatic deposition with pulsed rotation rates (Figures 4 and 5) provides additional non-steady state (or transient) information for the transport at however one applied current. For example, the supply rate of $Co(CHD)_2$ at the critical rotation speed directly corresponds to its incorporation rate. Quantification of impurity incorporation in the deposit could provide an estimation or confirmation of the diffusion coefficient of $Co(CHD)_2$. However, this is beyond the scope of this study, which focuses on the different behaviors of different molecules. Quantitative analysis and comparison of both studies will be needed in future to precisely assess the kinetic and transport parameters and allow numerical simulation for such deposition process.

3.3 Suppression speed

The amount of time it took for the suppression to take effect was measured by incrementally increasing the concentration of additives during galvanostatic deposition of cobalt. The potential transients in Figures 7 (a) and (b) represent the two different additives, CHD and CHO, respectively. In the case of CHD, the voltage increased immediately upon the injection showing that suppression effect is nearly instantaneous regardless of the current density used. The greatest change in suppression at -3 mA/cm^2 was observed upon the addition of 100 ppm CHD. Overshoot of suppression effect followed by relaxation of suppression was observed in some cases because of the stagnant flow of the injected concentrated additive solution and a locally high additive concentration immediately after the injection. When the concentration was further increased to 500 ppm a change of -50 mV was observed but the voltage did not increase as quickly. Additionally, when the concentration was increased by another 1,000 ppm (1500 ppm in total) the voltage varied greatly and did not stabilize at any particular value. This variation might be related to the catalytic hydrogen evolution reaction[36], where hydrogen bubbles on the electrode repeatedly block the surface.

The potential transient at -10mA/cm^2 was similar to the case of -3 mA/cm^2, where quick and strong suppression was observed. A maximum suppression of -150 mV was also observed at 300 ppm CHD. When the concentration was increased from 300 to 500 ppm the voltage did not change suggesting the suppression effect was saturated at 300 ppm. When the concentration was increased to 1,500 ppm the suppression did in fact increase again, however the increase was gradual. The mechanism of this gradual increase is not clear. 1500 ppm CHD is equivalent to 10.5 mM, which is still negligible in comparison with 0.3 M cobalt in the electrolyte. Therefore,

this can also reflect a partial blockage of the electrode surface by hydrogen bubbles or an additional suppression effect of the electrochemical kinetics on the electrode due to the presence of excessive CHD. Based on the stability constants in Table 1, the coordination between Co^{2+} with CHD is very stable. The additional CHD injected into the electrolyte was expected to form $[Co(CHD)_2]_{bulk}$ immediately upon injection. The rapid suppression reflects a fast adsorption behavior of $[Co(CHD)_2]_{bulk}$ onto electrode surface.

Injection of CHO into the electrolyte also resulted in suppression of cobalt deposition, but in a much less pronounced fashion. In both -3 and -10 mA/cm^2 trials of CHO the voltage did not significantly change until a concentration of 300 ppm was reached. While the suppression was fast, the magnitude was less than 30 mV. A small overshoot of potential increase was typically observed due to the stagnant nature of the additive dose before it got homogenized in the electrolyte. This is consistent with the little difference observed among the CVs with different concentrations of CHO. Additional injection of CHO to a concentration of 1500 ppm increased the voltage change up to 50 mV regardless of the current density used.

Again, the difference between CHD and CHO mainly lies in the presence and absence of a pair of oxime groups. It is obvious that Co-CHO chelate does not provide as strong suppressing effect on cobalt deposition as Co-CHD chelate. This could stem from either a weaker absorption or faster incorporation of such Co-CHD chelate. However, the fact that 1500 ppm CHO resulted in little suppression suggests a significantly weaker adsorption of the suppressing species is more likely to be the reason. On the other hand, the deposition behavior in presence of CHO in Figure 5(a) highly depended on electrode history indicates a very slow incorporation of the adsorbate.

3.4 Application point of view

From the point view of application for electrodeposition of cobalt interconnects, a strong, fast and yet controllable suppression effect is desired. During the electrodeposition of interconnect structures, the deeper the solution into the structure the less the agitation. When a rotation rate slightly above the critical rotation is used, the deposition will be fully suppressed at the top of trench and much less so at the bottom. This gradient of suppression across the depth of trench is desired for a preferential deposition at the trench bottom. The comparison between DMG, CHD and CHO clearly suggests a molecule with a pair of adjacent oxime groups, which typically forms a stable chelate with Co^{2+}, are necessary for the strong adsorption and thus a strong suppression. In addition, a bulky molecule with yet high enough solubility in electrolyte would be beneficial as well.

4. **Conclusion**

The effects of CHO and CHD on cobalt electrodeposition were studied and were compared with DMG from a previous study[34]. While all three additives showed some suppression effect on cobalt deposition, the lack of a pair of oxime groups in CHO resulted in a much weaker suppression. Both DMG and CHD showed S-shaped CVs at 100 ppm relating to a breakdown of suppression due to incorporation of the suppressing intermediates. A higher breakdown potential and a stronger suppression of CHD than DMG was believed to relate to the stronger coordination of CHD with Co^{2+}. An adsorbed chelate species such as $[Co(CHD)_2]_{ads}$ was proposed to involve in the suppression of cobalt deposition as well as a catalytic effect of hydrogen evolution. The breakdown of this adsorbed chelate relies on its formation, diffusion, adsorption, reduction and incorporation into deposit.

A critical rotation rate was defined in potentiostatic deposition with CHD. Full suppression and partial suppression were observed at rotation speeds above and below this critical value, respectively. Furthermore, the square root of critical rotation speed was found inversely proportional to CHD concentration, demonstrating an equilibrium between diffusion of $[Co(CHD)_2]_{bulk}$ and the incorporation of $[Co(CHD)_2]_{ads}$. On the other hand, the weak adsorption of CHO resulted in a suppression effect that is not only much weaker than CHD but dependent on the electrode history.

Acknowledgement

National science foundation is acknowledged for support through Grant CMMI-1662332. TL thanks Chenault Research Scholarship for travel support for research conference. Central analytical facility at the University of Alabama is acknowledged for help in some film characterization in this project.

References

1. D. Edelstein, J. Heidenreich, R. Goldblatt, W. Cote, C. Uzoh, N. Lustig, P. Roper, T. McDevitt, W. Motsiff, and A. Simon, *Full copper wiring in a sub-0.25 um CMOS ULSI technology.* Technical Digest of International Electron Devices Meeting, IEDM, 1997, **97**, 773.
2. P. Andricacos, C. Uzoh, J. Dukovic, J. Horkans, and H. Deligianni, *Damascene copper electroplating for chip interconnections.* IBM Journal of Research and Development, 1998, **42**(5), 567.
3. W. Steinhögl, G. Schindler, G. Steinlesberger, and M. Engelhardt, *Size-dependent resistivity of metallic wires in the mesoscopic range.* Physical Review B, 2002, **66**(7), 075414.
4. W. Wu, S.H. Brongersma, M. Van Hove, and K. Maex, *Influence of surface and grain-boundary scattering on the resistivity of copper in reduced dimensions.* Applied physics letters, 2004, **84**(15), 2838.
5. W. Zhang, S.H. Brongersma, O. Richard, B. Brijs, R. Palmans, L. Froyen, and K. Maex, *Influence of the electron mean free path on the resistivity of thin metal films.* Microelectronic Engineering, 2004, **76**(1-4), 146.
6. W. Zhang, S.H. Brongersma, Z. Li, D. Li, O. Richard, and K. Maex, *Analysis of the size effect in electroplated fine copper wires and a realistic assessment to model copper resistivity.* Journal of Applied Physics, 2007, **101**(6), 063703.
7. K. Barmak, A. Darbal, K.J. Ganesh, P.J. Ferreira, J.M. Rickman, T. Sun, B. Yao, A.P. Warren, and K.R. Coffey, *Surface and grain boundary scattering in nanometric Cu thin films: A quantitative analysis including twin boundaries.* Journal of Vacuum Science & Technology A, 2014, **32**(6), 061503.

8. R.L. Graham, G.B. Alers, T. Mountsier, N. Shamma, S. Dhuey, S. Cabrini, R.H. Geiss, D.T. Read, and S. Peddeti, *Resistivity dominated by surface scattering in sub-50 nm Cu wires.* Applied Physics Letters, 2010, **96**(4).

9. D. Gall, *Electron mean free path in elemental metals.* Journal of Applied Physics, 2016, **119**(8), 085101.

10. J. Kelly, J.-C. Chen, H. Huang, C. Hu, E. Liniger, R. Patlolla, B. Peethala, P. Adusumilli, H. Shobha, and T. Nogami. *Experimental study of nanoscale Co damascene BEOL interconnect structures*. in *2016 IEEE International Interconnect Technology Conference - Advanced Metallization Conference (IITC/AMC)*, 40, 2016, San Jose, CA.

11. C.-C. Wei, E. Chou, S. Shih, and S.-M. Lin. *Bottom-up Filling of Damascene Trenches with Cobalt By Electroplating Process*. in *228th Electrochemical Society Meeting Abstract*, 949, 2015, Phoenix, AZ.

12. T.P. Moffat, D. Wheeler, W.H. Huber, and D. Josell, *Superconformal Electrodeposition of Copper.* Electrochemical and Solid-State Letters, 2001, **4**, C26.

13. A.C. West, S. Mayer, and J. Reid, *A Superfilling Model that Predicts Bump Formation.* Electrochemical and Solid-State Letters, 2001, **4**, C50.

14. T. Moffat, D. Wheeler, M. Edelstein, and D. Josell, *Superconformal film growth: mechanism and quantification.* IBM Journal of Research and Development, 2005, **49**(1), 19.

15. J. Kelly and A. West, *Copper Deposition in the Presence of Polyethylene Glycol - I. Quartz Crystal Microbalance Study.* Journal of The Electrochemical Society, 1998, **145**, 3472.

16. J. Kelly and A. West, *Copper Deposition in the Presence of Polyethylene Glycol - II. Electrochemical Impedance Study.* Journal of The Electrochemical Society, 1998, **145**, 3477.

17. T.P. Moffat, J.E. Bonevich, W.H. Huber, A. Stanishevsky, D.R. Kelly, G.R. Stafford, and D. Josell, *Superconformal Electrodeposition of Copper in 500–90 nm Features.* Journal of The Electrochemical Society, 2000, **147**, 4524.

18. P. Vereecken, R. Binstead, H. Deligianni, and P. Andricacos, *The chemistry of additives in damascene copper plating.* IBM Journal of Research and Development, 2005, **49**(1), 3.

19. R. Akolkar and U. Landau, *A Time-Dependent Transport-Kinetics Model for Additive Interactions in Copper Interconnect Metallization.* Journal of The Electrochemical Society, 2004, **151**, C702.

20. R. Akolkar and U. Landau, *Mechanistic Analysis of the Bottom-Up Fill in Copper Interconnect Metallization.* Journal of The Electrochemical Society, 2009, **156**, D351.

21. Q. Huang, B.C. Baker-O'Neal, J.J. Kelly, P. Broekmann, A. Wirth, C. Emnet, M. Martin, M. Hahn, A. Wagner, and D. Mayer, *Suppressor Effects during Copper Superfilling of Sub-100 nm Lines.* Electrochemical and Solid-State Letters, 2009, **12**(4), D27.

22. Q. Huang, J. Liu, and B.C. Baker-O'Neal, *An Electrochemical Method of Suppressor Screening for Cu Plating in Sub-100 nm Lines.* Journal of The Electrochemical Society, 2014, **161**(5), D207.

23. D. Josell, B. Baker, C. Witt, D. Wheeler, and T. Moffat, *Via filling by electrodeposition superconformal silver and copper and conformal nickel.* Journal of the Electrochemical Society, 2002, **149**(12), C637.

24. B. Baker, C. Witt, D. Wheeler, D. Josell, and T. Moffat, *Superconformal silver deposition using KSeCN derivatized substrates.* Electrochemical and solid-state letters, 2003, **6**(5), C67.

25. D. Josell, C. Beauchamp, D. Kelley, C. Witt, and T. Moffat, *Gold superfill in sub-micrometer trenches.* Electrochemical and solid-state letters, 2005, **8**(3), C54.

26. S. Kim, J. Bonevich, D. Josell, and T. Moffat, *Electrodeposition of Ni in Submicrometer Trenches.* Journal of The Electrochemical Society, 2007, **154**, D443.

27. C.H. Lee, J.E. Bonevich, J.E. Davies, and T.P. Moffat, *Magnetic Materials for Three-Dimensional Damascene Metallization: Void-Free Electrodeposition of Ni and Ni70Fe30 Using 2-Mercapto-5-benzimidazolesulfonic Acid.* Journal of The Electrochemical Society, 2008, **155**(7), D499.

28. C.H. Lee, J.E. Bonevich, J.E. Davies, and T.P. Moffat, *Superconformal Electrodeposition of Co and Co-Fe Alloys Using 2-Mercapto-5-benzimidazolesulfonic Acid.* Journal of the Electrochemical Society, 2009, **156**(8), D301.

29. C.H. Lee, J.E. Bonevich, U. Bertocci, K.L. Steffens, and T.P. Moffat, *Superconformal Ni Electrodeposition Using 2-Mercaptobenzimidazole.* Journal of The Electrochemical Society, 2011, **158**(6), D366.

30. D. Josell and T.P. Moffat, *Superfilling Damascene Trenches with Gold in a Sulfite Electrolyte.* Journal of The Electrochemical Society, 2013, **160**(12), D3009.

31. D. Josell, M. Silva, and T.P. Moffat, *Superconformal Bottom-up Cobalt Deposition in High Aspect Ratio through Silicon Vias.* Journal of The Electrochemical Society, 2016, **163**(14), D809.

32. D. Josell and T. Moffat, *Superconformal Bottom-Up Nickel Deposition in High Aspect Ratio Through Silicon Vias.* Journal of The Electrochemical Society, 2016, **163**(7), D322.

33. D. Liang, J. Liu, K. Reuter, B. Baker-O'Neal, and Q. Huang, *Electroplating of Fe-Rich NiFe Alloys in Sub-50 nm Lines.* Journal of the Electrochemical Society, 2014, **161**(5), D301.

34. Q. Huang, T. Lyons, and W. Sides, *Electrodeposition of Cobalt for Interconnect Application: Effect of Dimethylglyoxime.* Journal of The Electrochemical Society, 2016, **163**(13), D715.

35. V. Fourmond, P.-A. Jacques, M. Fontecave, and V. Artero, *H2 evolution and molecular electrocatalysts: determination of overpotentials and effect of homoconjugation.* Inorganic chemistry, 2010, **49**(22), 10338.

36. N. Kaeffer, M. Chavarot-Kerlidou, and V. Artero, *Hydrogen Evolution Catalyzed by Cobalt Diimine–Dioxime Complexes.* Accounts of chemical research, 2015, **48**(5), 1286.

37. N. Kaeffer, A. Morozan, J. Fize, E. Martinez, L. Guetaz, and V. Artero, *The Dark Side of Molecular Catalysis: Diimine–Dioxime Cobalt Complexes Are Not the Actual Hydrogen Evolution Electrocatalyst in Acidic Aqueous Solutions.* ACS Catalysis, 2016, **6**(6), 3727.

38. Z.Q. Wang, L.Z. Tang, Y.X. Zhang, S.Z. Zhan, and J.S. Ye, *Electrochemical-driven water splitting catalyzed by a water-soluble cobalt(II) complex supported by N,N '-bis(2 '-pyridinecarboxamide)-1,2-benzene with high turnover frequency.* Journal of Power Sources, 2015, **287**, 50.

39. D. Roha and U. Landau, *Mass Transport of Leveling Agents in Plating: Steady-State Model for Blocking Additives.* Journal of The Electrochemical Society, 1990, **137**(3), 824.

40. Y.-J. Li, J. Oslonovitch, N. Mazouz, F. Plenge, K. Krischer, and G. Ertl, *Turing-type patterns on electrode surfaces.* Science, 2001, **291**(5512), 2395.

41. T. Moffat and D. Josell, *Extreme bottom-up superfilling of through-silicon-vias by damascene processing: suppressor disruption, positive feedback and turing patterns.* Journal of The Electrochemical Society, 2012, **159**(4), D208.

42. A.E. Martell and R.M. Smith, *Critical stability constants*. 1974: Springer.

43. V.G. Levich, *Physicochemical hydrodynamics*. 1962: Prentice Hall.

Table 1. Molecular weights of the three additives with breakdown of oxime and alkyl groups, the stability constants of the chelates with Ni^{2+}, and the calculated shifts of reversible potential due to the chelating.

(g/mol)	molecular weight	oxime groups	side alkyl groups	oxime weight %	alkyl weight %	$pK_{s.t.}$	ΔE_{rev}
DMG	116	86	30	74%	26%	17.2	-0.500 V
CHD	142	86	56	61%	39%	21.5	-0.625 V
CHO	113	43	70	38%	62%	NA	NA

Figure captions

Figure 1. Molecular structures of dimethylglyoxime (DMG), cyclohexane dioxime (CHD), and cyclohexane oxime (CHO).

Figure 2. Cyclic voltammetry of cobalt electrodeposition on RDE at 100 rpm in presence of (a) CHD and (b) CHO at various concentrations.

Figure 3. The comparison of the polarization (forward scan of CV) of cobalt electrodeposition on RDE at 100 rpm in presence of DMG, CHD and CHO at (a) 100 ppm and (b) 300 ppm in comparison with additive free case.

Figure 4. Potentiostatic cobalt deposition on RDE at -0.95 V in presence of (a) 100 ppm and (b) 71 ppm CHD with various rotation speeds, and (c) the inversely proportional relation between the square root of critical rotation rates and CHD concentrations.

Figure 5. Potentiostatic cobalt deposition on RDE at (a) -0.85 V and (b) -0.815 V in presence of 100 ppm CHO with various rotation speeds. Inset in (b) shows the relation between steady state current densities and square root of rotation rates.

Figure 6. Cyclic voltammetry of 100 ppm (a) CHD and (b) CHO at 100, 400, and 900 ppm rotation rates. CV without any additives at 100 rpm was also presented for comparison.

Figure 7. Galvanostatic cobalt deposition on RDE at 100 rpm with incremental injection of (a) CHD and (b) CHO at (a1, b1) -3 mA/cm^2 and (a2, b2) -10 mA/cm^2.

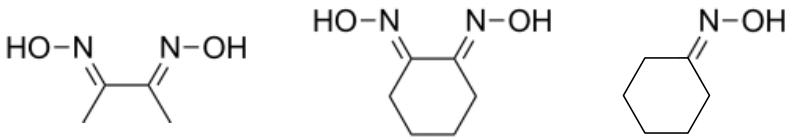

Dimethylglyoxime (DMG) | 1,2-Cyclohexanedione dioxime (CHD) | Cyclohexanone oxime (CHO)

Figure 1

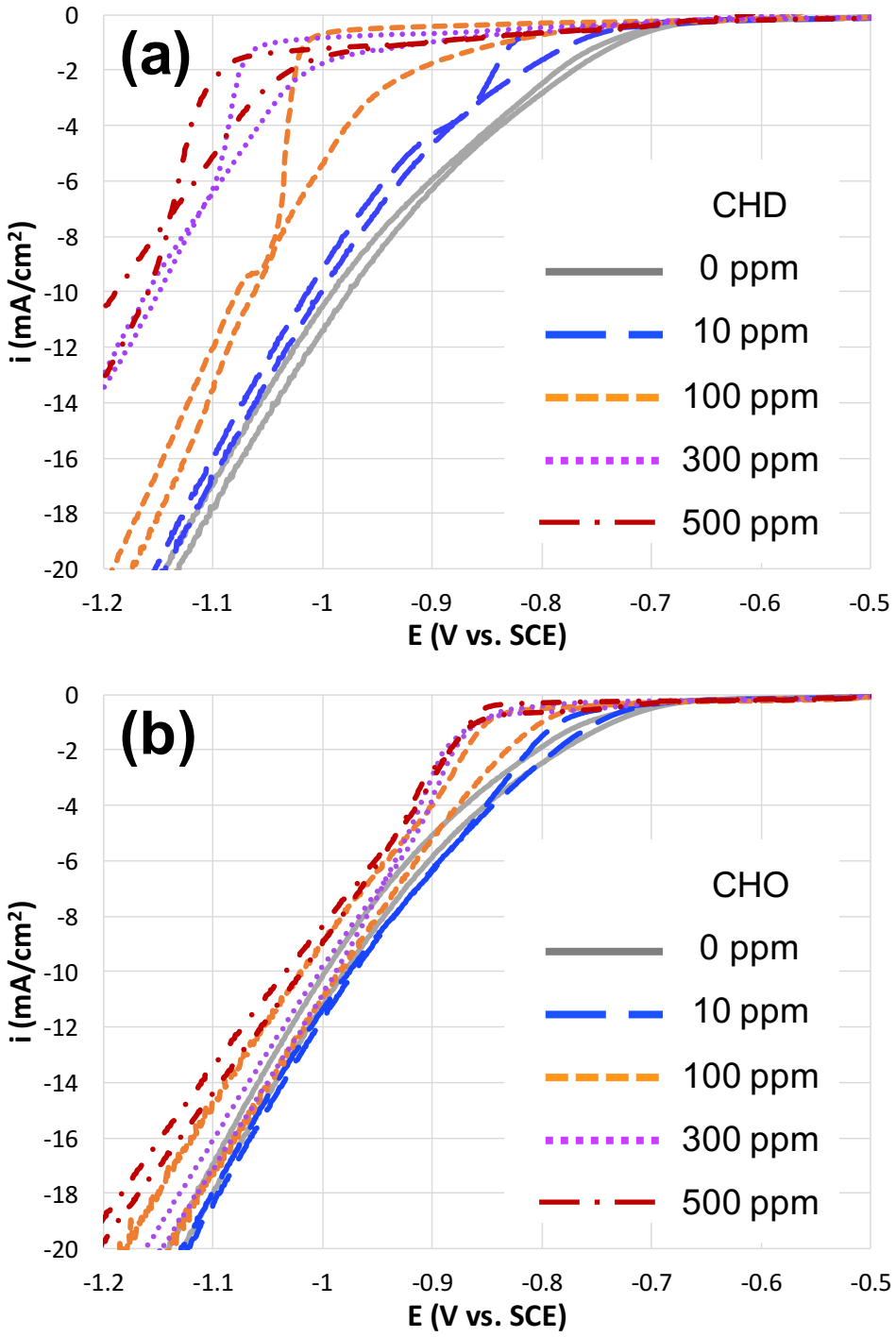
(a)
i (mA/cm²)
E (V vs. SCE)
CHD
0 ppm
10 ppm
100 ppm
300 ppm
500 ppm
(b)
i (mA/cm²)
E (V vs. SCE)
CHO
0 ppm
10 ppm
100 ppm
300 ppm
500 ppm

Figure 2

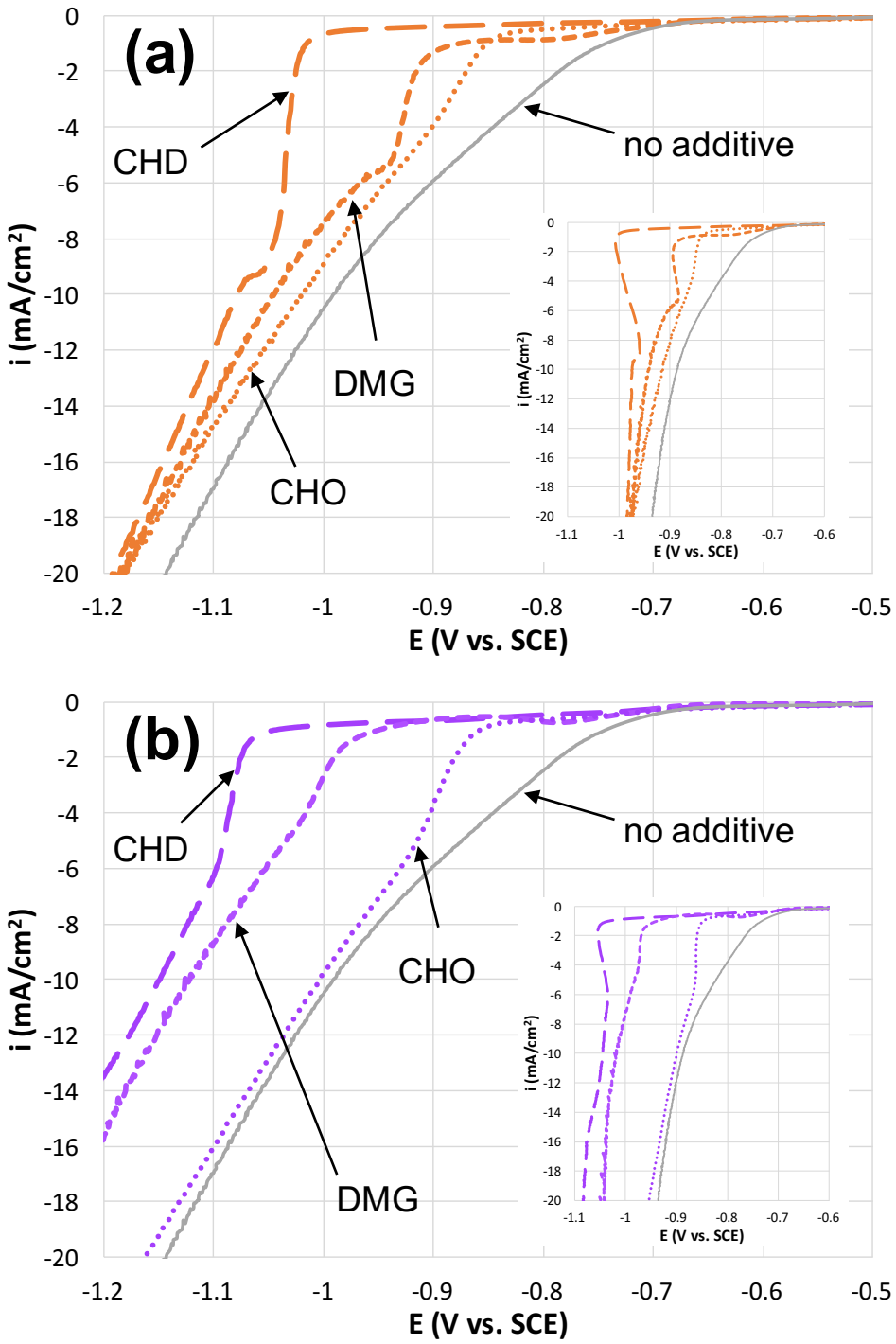
(a)
CHD
no additive
DMG
CHO
i (mA/cm²)
E (V vs. SCE)
(b)
CHD
no additive
CHO
DMG
i (mA/cm²)
E (V vs. SCE)

Figure 3

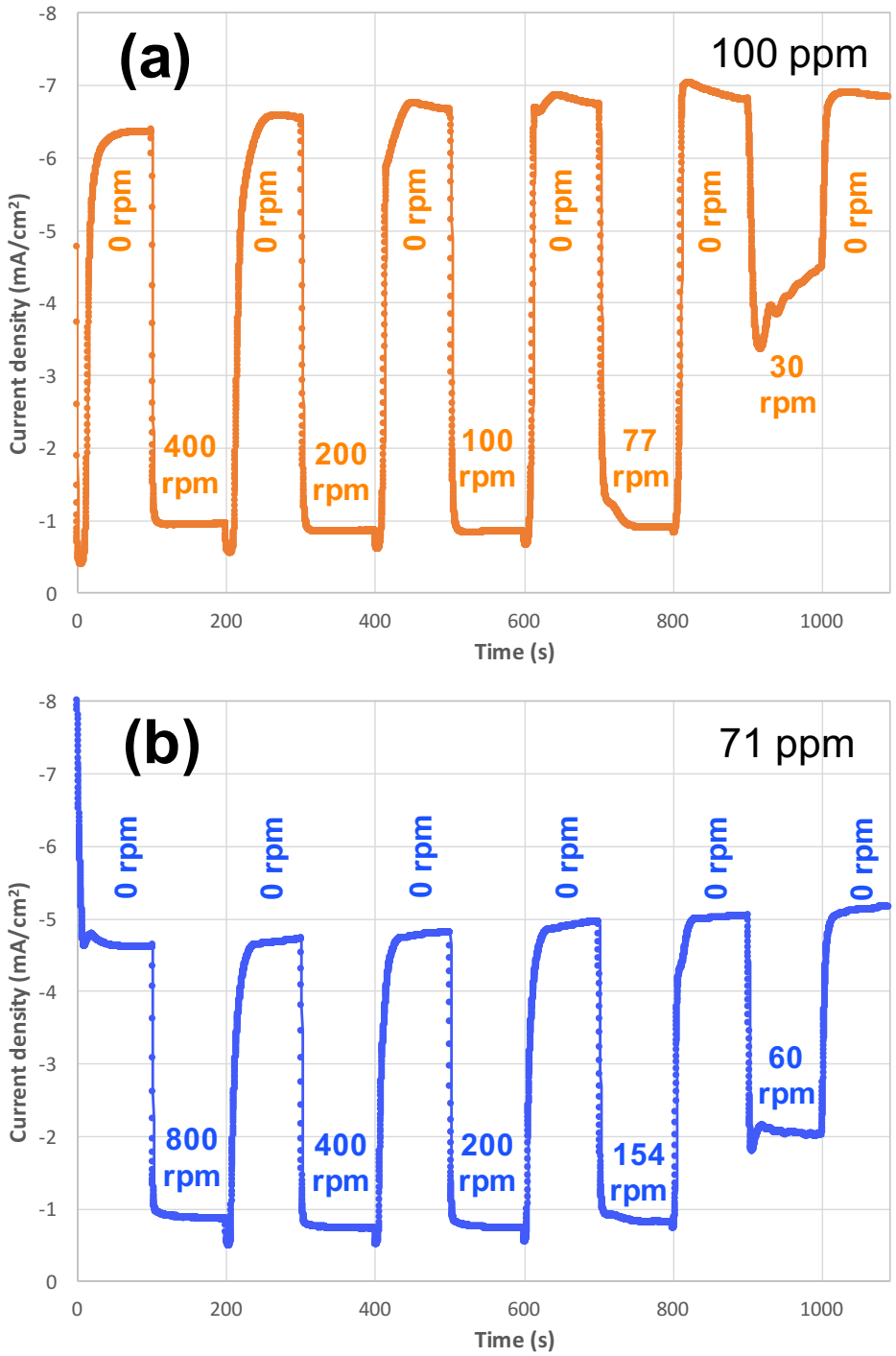
(a)
100 ppm
0 rpm
400 rpm
200 rpm
100 rpm
77 rpm
30 rpm
Current density (mA/cm²)
Time (s)
(b)
71 ppm
0 rpm
800 rpm
400 rpm
200 rpm
154 rpm
60 rpm
Current density (mA/cm²)
Time (s)

Figure 4

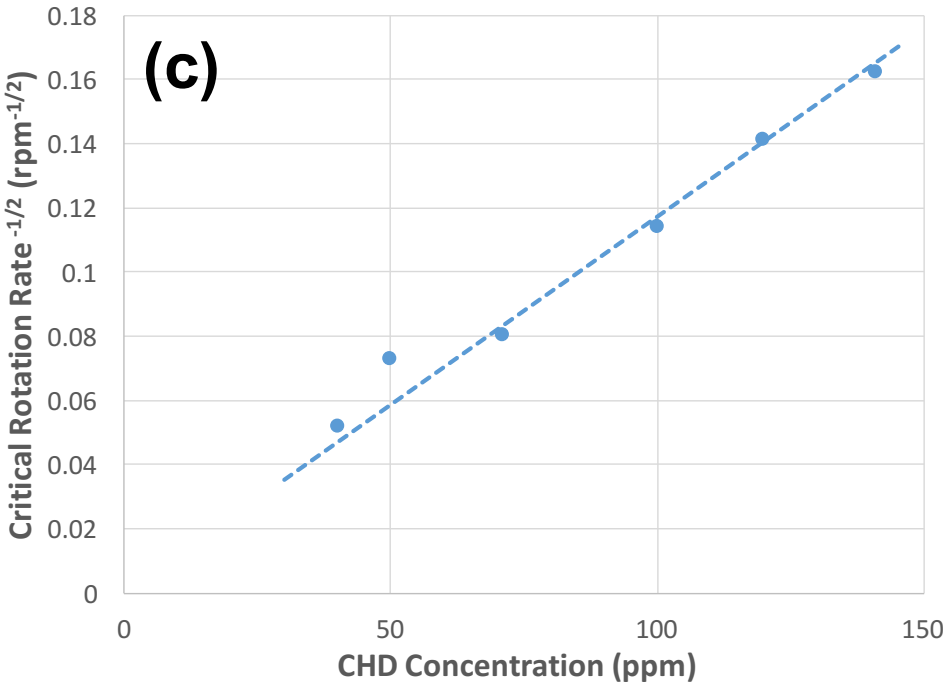
(c)
Critical Rotation Rate -1/2 (rpm-1/2)
0.18
0.16
0.14
0.12
0.1
0.08
0.06
0.04
0.02
0
0
50
100
150
CHD Concentration (ppm)

Figure 4

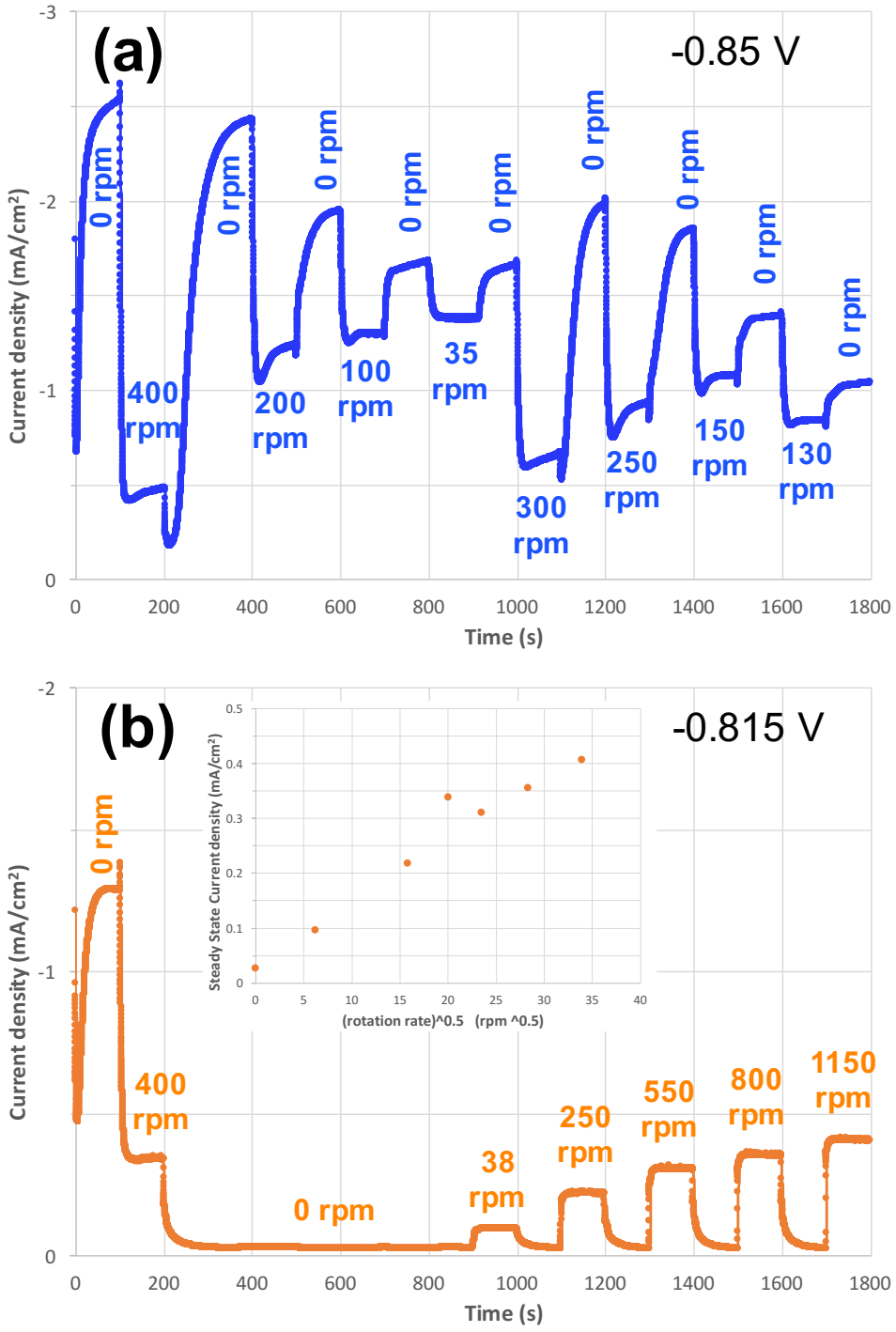
(a)
-0.85 V
Current density (mA/cm²)
Time (s)
0 rpm
400 rpm
200 rpm
100 rpm
35 rpm
300 rpm
250 rpm
150 rpm
130 rpm
(b)
-0.815 V
Steady State Current density (mA/cm²)
(rotation rate)^0.5 (rpm ^0.5)
38 rpm
550 rpm
800 rpm
1150 rpm

Figure 5

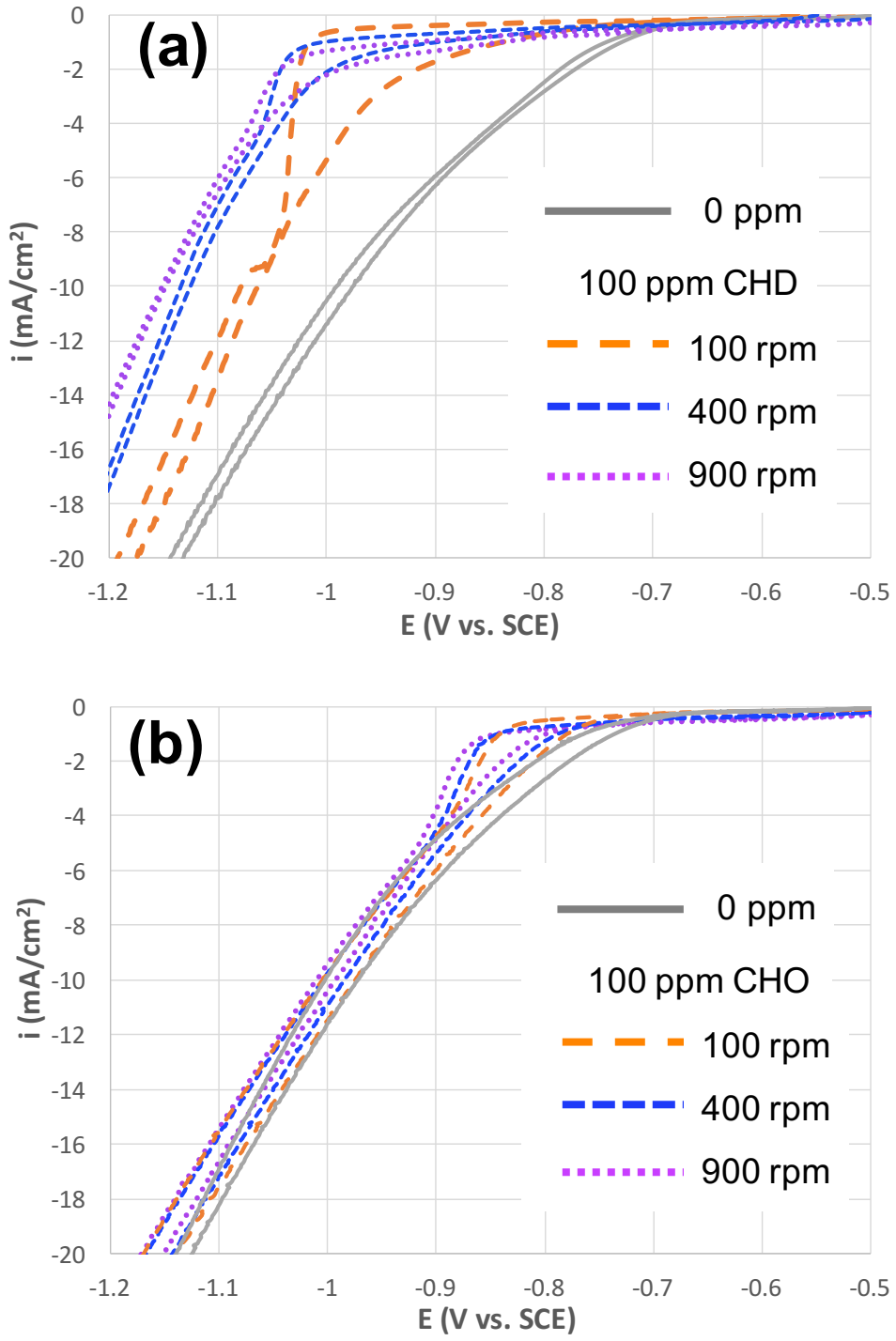
(a)
0
-2
-4
-6
-8
-10
-12
-14
-16
-18
-20
i (mA/cm²)
-1.2
-1.1
-1
-0.9
-0.8
-0.7
-0.6
-0.5
E (V vs. SCE)
0 ppm
100 ppm CHD
100 rpm
400 rpm
900 rpm
(b)
0
-2
-4
-6
-8
-10
-12
-14
-16
-18
-20
i (mA/cm²)
-1.2
-1.1
-1
-0.9
-0.8
-0.7
-0.6
-0.5
E (V vs. SCE)
0 ppm
100 ppm CHO
100 rpm
400 rpm
900 rpm

Figure 6

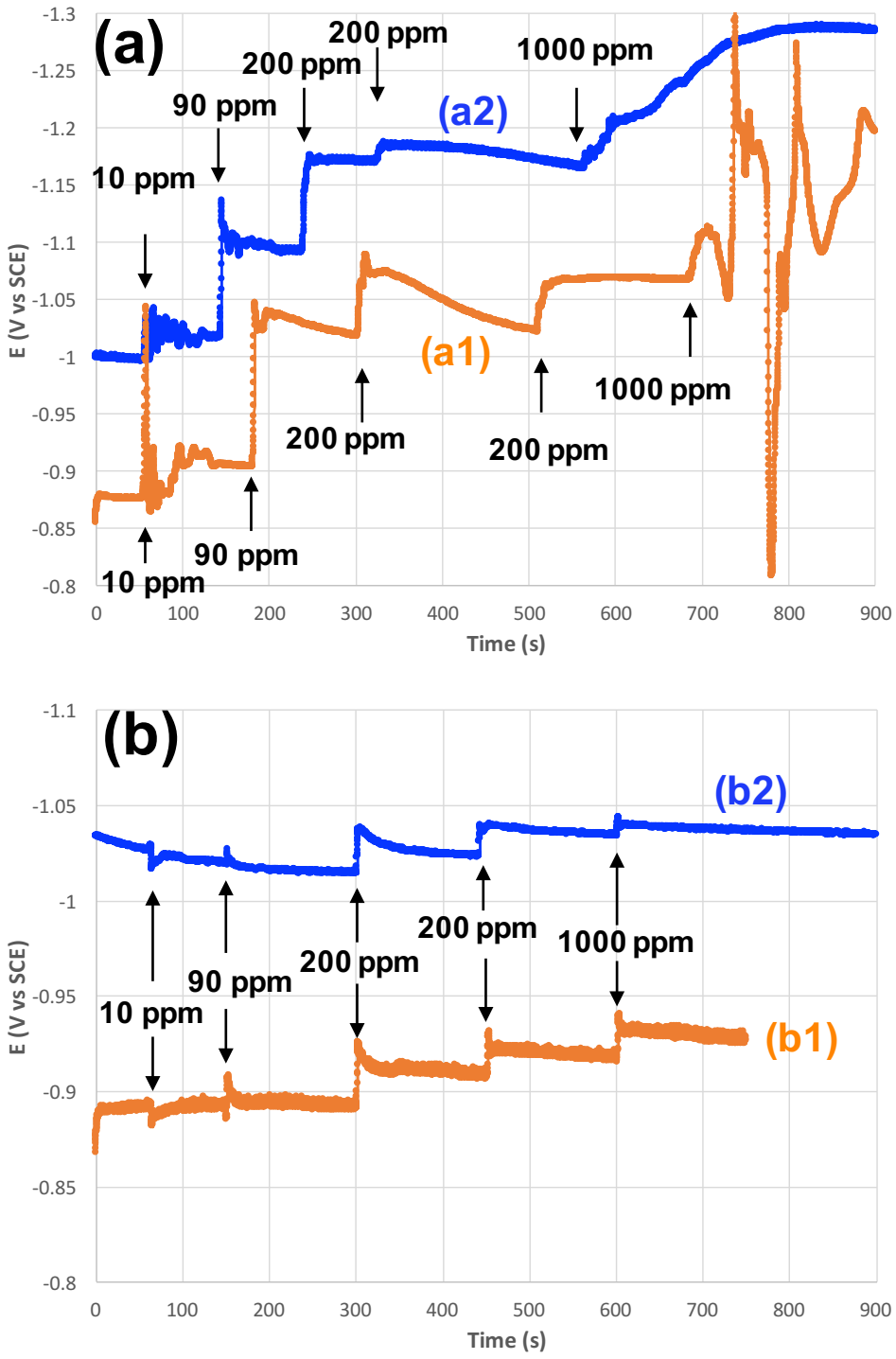
(a)
200 ppm
200 ppm
1000 ppm
90 ppm
(a2)
10 ppm
(a1)
1000 ppm
200 ppm
200 ppm
90 ppm
10 ppm
E (V vs SCE)
Time (s)
(b)
(b2)
200 ppm
1000 ppm
90 ppm
200 ppm
10 ppm
(b1)
E (V vs SCE)
Time (s)

Figure 7